Nonlinear Resonance Effects in a Linear Paul Trap

Ryota TAKAI*, Kenji NAKAYAMA, Wataru SAIKI, Kiyokazu ITO and Hiromi OKAMOTO

Department of Quantum Matter, Graduate School of Advanced Sciences of Matter, Hiroshima University, 1-3-1 Kagamiyama, Higashi-Hiroshima, Hiroshima 739-8530, Japan

The effects of nonlinear resonances in a linear Paul trap have been investigated through systematic experiments and numerical simulations. The main causes of the nonlinearity that affects the stability of the ion motion are the use of circular (rather than hyperbolic) electrodes, their misalignments, and Coulomb interactions among the ions. A particle tracking code based on a two-dimensional model is employed to study the efficiency of plasma storage and to confirm the existence of nonlinear resonance stop bands. Experiments are performed with Ar^+ plasmas that are eventually detected by a Faraday cup after a short storage. The obtained data are compared with numerical simulations in which the exact three-dimensional structure of the trap system has been incorporated. Several nonlinear stop bands have been experimentally identified inside the Mathieu stability region. It is demonstrated that the location of a resonance stop band moves due to the space-charge potential depending on the number of confined ions.

KEYWORDS: nonlinear resonance, one-component plasma, linear Paul trap, space charge effect, charged particle beam

1. Introduction

Since the invention of a quadrupole mass filter by Paul in 1953,[1] compact radio-frequency (rf) devices that guide and confine low-energy charged particles have become increasingly common in physics, chemistry, biology, vacuum technologies, space and environment sciences. The three-dimensional (3D) confinement of ion clouds can readily be achieved by an rf quadrupole system that is often referred to as a Paul trap after the inventor. In 1989, Prestage and coworkers developed the first *linear Paul trap* by axially closing the mass filter with electrostatic potentials.[2] Since the rf field in this type of trap disappears along the axis, it is possible to confine a large number of ions with relatively small disturbance from the time-dependent potential. Linear Paul traps, equipped with a laser cooler, have now been utilized for diverse experimental purposes related to frequency standards,[3–5] high-resolution spectroscopy,[6,7] optical mass spectrometry,[8,9] ion/molecule reactions,[10–12] and Coulomb crystallization.[13–15] For the last decade, a Coulomb crystallized string of ions has been studied as one of promising candidates for quantum information processors.[16–23]

Recently, Okamoto and Tanaka proposed a unique application of a Paul trap for the study of beam physics.[24–26] The idea is based on the fact that the collective motion of a charged particle beam is approximately equivalent to that of a one-component plasma confined in the trap. Following this idea, we have constructed a table-top system "S-POD (Simulator for Particle Orbit Dynamics)" to explore various collective effects in space-charge-dominated beams.[27,28] In order to experimentally simulate the collective dynamics of an intense beam traveling in an accelerator, it is necessary to store as many ions as possible for a sufficiently long period. Among possible undesirable effects that may lead to a rapid loss of particles, *nonlinear resonance* is one of the most influential. In the present case, resonant instability is caused parametrically by various imperfection sources contained in the actual trap structure. If the operating point of the trap is not properly chosen, the storage time of the plasma is considerably shortened. It is thus important to set the operating point away from critical resonances.

The effect of nonlinear resonances in a mass filter was first discussed by von Busch and Paul in 1961.[29] Their work was extended by Dawson and Whetten who experimentally demonstrated the occurrence of resonances in a Paul trap.[30] After these pioneering works, many theoretical and experimental studies on nonlinear resonances in two-dimensional (2D) mass filters or conventional Paul traps have been performed mainly in connection with the splitting of mass peaks.[31–40] However, regarding linear Paul traps, little has been done so far except for a few experimental reports on small laser-cooled ion clouds.[41,42]

In this paper, we present experimental results on nonlinear resonances in a linear Paul trap confining a relatively large number of ions. After summarizing the theoretical backgrounds of this phenomenon in §2, experimental observations are shown in §3 which verify the existence of parametric resonances of various orders and their dependence on the Coulomb potential. The multisection linear Paul trap for S-POD[28] was used for the experiments. The results are compared with numerical data obtained with a 3D particle tracking code that simulates the ion motion in the actual confinement fields.

2. Theoretical Considerations

2.1 Nonlinear resonance conditions

Transverse resonances in a linear Paul trap can be described by the 2D theory originally developed for quadrupole mass filters.[35,36] Since various imperfection fields are inevitable in practice, the linear Mathieu equation is not relevant to the correct description of parti-

*E-mail address: takai@hiroshima-u.ac.jp

cle orbits in the trap. The nonlinear fields come mainly from non-hyperbolic electrode surfaces, fabrication errors, field distortion in the edge regions, insulator charging, noises in applied voltages, and space-charge interactions. In the 2D model, the general scalar potential including these nonlinear perturbations can be written, in the cylindrical coordinates (r, θ), as

$$\phi(r,\theta,t) = (U + V\cos\Omega t)\sum_{n=0}^{\infty} C_n \left(\frac{r}{R}\right)^n \cos n\theta, \qquad (1)$$

where U and V are the dc bias potential and rf amplitude, Ω is the angular rf frequency, R is the minimum distance from the trap axis to the surface of the quadrupole rods, and C_n's are the dimensionless weight factor depending on the relative strengths of the linear and nonlinear terms. In what follows, the quadrupole coefficient, which is much greater than any other coefficients, is normalized to be unity by scaling U and V; namely, we put $C_2 = 1$ without loss of generality. When the higher-order coefficients are finite, the horizontal and vertical motions of particles are no longer independent but coupled to each other.

Although the ideal surface of the quadrupole electrodes should be hyperbolic, we often employ cylindrical electrodes that considerably simplify the manufacture and fabrication of the trap. This simplification inevitably yields an additional imperfection in the plasma confinement field. Provided that the electrodes are perfectly aligned and thus the system holds four-fold symmetry, only limited harmonics with $n = 2, 6, 10, \cdots$ appear. In order to minimize the first nonlinear component, i.e. the dodecapole C_6, the radius ρ of the electrodes is chosen such that $\rho/R = 1.14511$.[43–45] Our Paul trap actually uses cylindrical electrodes whose radius is $1.15R$.

The general resonance condition of order N is given by[35,36]

$$n_x\beta_x + n_y\beta_y = 2k \quad (|n_x| + |n_y| = N) \qquad (2)$$

where n_x, n_y and k are all integers, and $\beta_{x(y)}$ is the characteristic exponent of the solution of the Mathieu equation depending on the so-called Mathieu parameters a and q. $\beta_{x(y)}$ takes a value between 0 and 1 in the first stable region of the Mathieu diagram, and can be related to the angular frequency $\omega_{x(y)}$ of the secular motion as $\beta_{x(y)} = 2\omega_{x(y)}/\Omega$. When a driving nonlinear term has order n, the resultant resonances are particularly strong for $N = n, n-2, n-4, \cdots, 4$ or 3.[35,36] As is well-known, the energy of the x direction (horizontal) and that of the y direction (vertical) are exchanged under a difference resonance ($n_x n_y < 0$) while preserving the total energy. In the other cases where $n_x n_y \geq 0$, the particles absorb energy from the driving rf field and, accordingly, the amplitude of the secular oscillation increases. The secular frequency, however, eventually goes out of the resonance due to its dependence on the oscillation amplitude. As a result, the resonant particles execute a sort of beat motions. This means that whether a particle is lost or not depends on the maximum amplitude of the beat oscillation; namely, particles that have the amplitudes greater than R will be lost. In the following, we only consider the latter type of resonances because it should more seriously affect the storage time of a confined plasma.

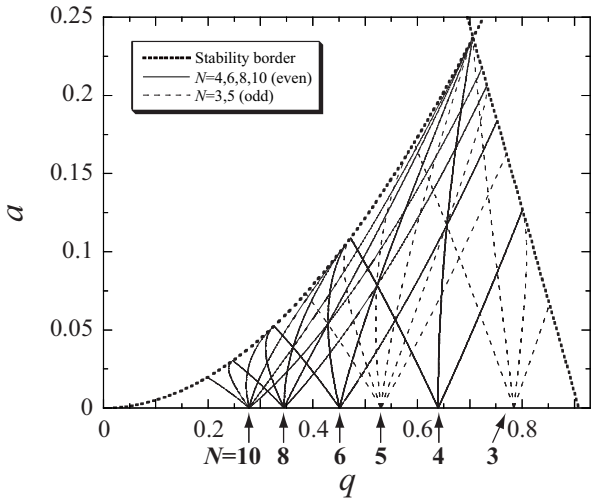

Fig. 1. The first stability region of the Mathieu equation. Nonlinear resonance lines predicted by eq. (2) with $k = 1$ have been indicated by solid and broken curves.

The resonance lines derived from eq. (2) are plotted in Fig. 1 that suggests the possibility of various nonlinear resonances even when the operating point is well inside the Mathieu stability region. Each line is accompanied by an instability domain (stop band) with a finite width depending on the strength of the driving force, in other words, on the magnitude of C_n. The weight factor C_n generally becomes smaller for a larger n. In the present example, we have put $k = 1$ and drawn resonance lines for $N = 3, 4, 5, 6, 8, 10$. Several lines of a specific order have converged at a single point on the q-axis. It is also evident from eq. (2) that a low-order resonance overlaps with many higher-order resonances.

2.2 2D tracking simulations

Before proceeding to experimental observations, we here make a brief numerical study of nonlinear resonances in a linear Paul trap, employing a simple 2D model. Assuming the general potential in eq. (1), the transverse equation of motion of a confined particle with rest mass m and charge state Q is expressed in Cartesian coordinates as

$$\frac{d^2u}{d\xi^2} \pm (a + 2q\cos 2\xi)\, u = -\frac{4Q}{m\Omega^2}\frac{\partial \phi'}{\partial u}, \qquad (3)$$

where $a \equiv 8QU/(mR^2\Omega^2)$ and $q \equiv 4QV/(mR^2\Omega^2)$ are the Mathieu parameters, $\xi \equiv \Omega t/2$ is the dimensionless independent variable, the scalar potential ϕ' includes all multipole components except for quadrupole, i.e. the $n \geq 3$ terms in eq. (1), and u denotes either the horizontal coordinate x or vertical coordinate y. In order to estimate the efficiency of plasma storage, we have numerically integrated eq. (3) with possible combinations of a and q in the first Mathieu stability region. In our current system, single-species plasmas are generated by ionizing neutral gases with low-energy electrons from an electron gun sitting outside the Paul trap. We expect that ions

are produced not only near the axis but also almost everywhere in the plasma confinement region. Considering this fact, test particles were randomly distributed within the circle of radius R_0 ($< R$) at the beginning of each simulation. The momentum distributions were chosen to be Gaussian in both transverse degrees of freedom. The standard deviation of the Gaussian can be determined from plasma temperature T. If the oscillation amplitude of a particle exceeds the radius R of the plasma confinement space, that particle is considered to be lost. The storage efficiency is evaluated from the number of survived particles after 1000 rf periods.

2.2.1 *Pure quadrupole confinement*

We start from the ideal case where the plasma confinement field is pure quadrupole, i.e. $\phi' = 0$. Figure 2 shows the storage efficiencies of two typical cases; a relatively low temperature plasma has been assumed in the upper picture while, in the lower picture, we have set the initial temperature of a plasma twice higher and the transverse extent halved. The numbers of survived particles obtained in a set of many simulations along a particular *mass scan line* $a = (2U/V)q$ have been normalized by the peak value. Therefore, the normalized efficiencies in Fig. 2 do not necessarily reflect the absolute number of survived particles relative to the initial particle number. The transverse extent of a stationary plasma calculated from the envelope equation becomes minimum along the broken curve.[28] If it is possible to provide well-conditioned plasmas initially, this curve determines the optimum operating parameters with which the number of confinable ions can be maximized. In the case of Fig. 2(a), the region of high storage efficiency has been significantly shifted to the left because of the initial mismatch of the particle distribution. The hatched area approaches and eventually covers the broken curve at higher temperature when the plasma extent is fixed at $R_0 = 0.8R$. In contrast, the hatched area in Fig. 2(b) moves leftward if we increase R_0 while keeping T. Since the horizontal and vertical motions are linear and decoupled, these numerical results can readily be explained by checking the amount of phase-space mismatch between the initial particle distribution and the transverse acceptance of the trap.

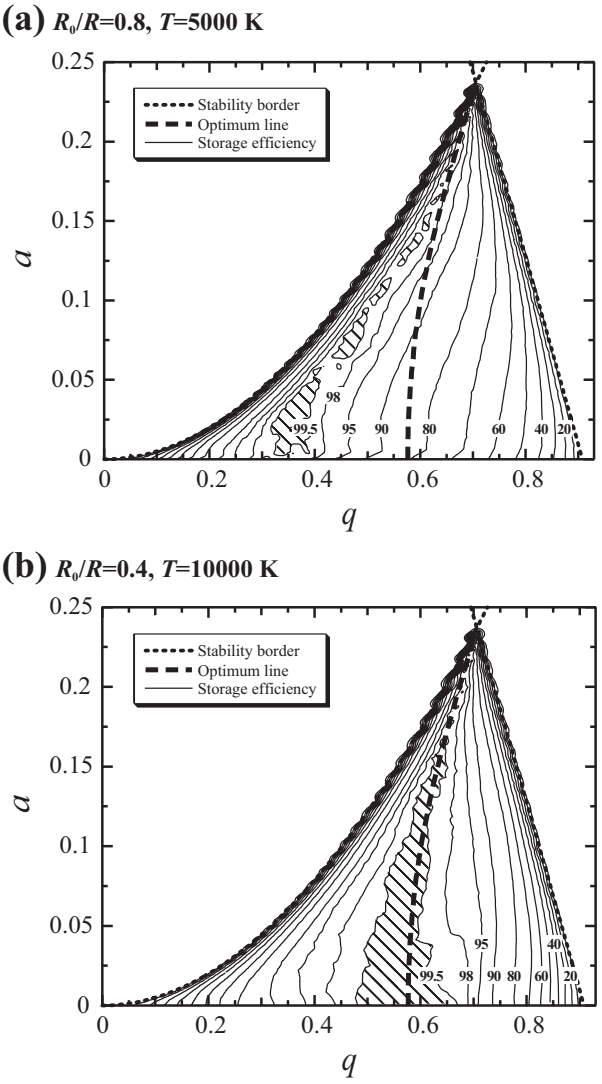

Fig. 2. Contour plots of storage efficiencies (in percentage) estimated from 2D tracking simulations. The pure quadrupole confinement field has been assumed. The initial conditions adopted for the two examples are: (a) $R_0/R = 0.8$ and $T = 5000$ K, (b) $R_0/R = 0.4$ and $T = 10000$ K. Storage efficiencies are evaluated from many simulations performed along many different *mass scan lines*; they have been normalized by the maximum number of survived particles in each set of simulations along a specific mass scan line. The broken curve is the theoretically obtained "optimum" operating line along which the transverse extent of a stationary plasma can be minimized.

2.2.2 *Confinement with error fields*

We now take into account the contribution from the nonlinear perturbing terms in eq. (3). Since the major source of nonlinearity expected in our Paul trap is the non-hyperbolic shape of the electrodes, we turn on the $n = 6$ and $n = 10$ terms, both of which have the same strengths, i.e. $C_6 = C_{10} = -0.01$. Results of systematic simulations are summarized in Fig. 3 where shadow has been deepened in proportion to the number of survived particles. The initial extent and temperature of plasmas have been set at $R_0 = 0.8R$ and $T = 5000$ K in all simulations. We find several narrow bands in which the loss rate of particles is particularly enhanced. Comparison of Fig. 3 with Fig. 1 enables us to conclude that these losses are caused by nonlinear resonances under the conditions $\beta_x + \beta_y/2 = 1$ ($N = 3$), $2\beta_x = 1$, $\beta_x + \beta_y = 1$, $2\beta_y = 1$ ($N = 4$), $2\beta_x + \beta_y = 1$, $\beta_x + 2\beta_y = 1$ ($N = 6$). Figure 4 shows the Poincaré plots obtained from the simulation data at the operating points A and B in Fig. 3. We recognize the formation of six islands in the left panel and four islands in the right panel, which proves that the nonlinear resonances with $N = 6$ and $N = 4$ are responsible for the particle losses at A and B.

2.3 *Possible shift of stop bands*

There are several factors that may give rise to noticeable shifts of resonance stop bands from the locations predicted by the single-particle theory for 2D mass filters (Fig. 1):

(i) Static potential for axial plasma confinement

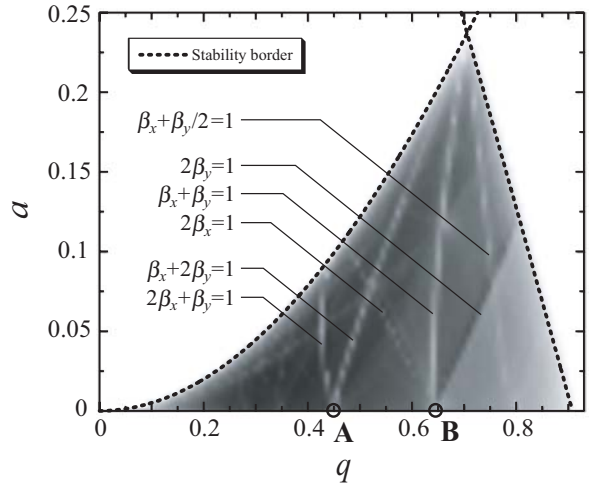

Fig. 3. Loss rate of confined particles evaluated from 2D tracking simulations. In addition to the dominant quadrupole field, the nonlinear fields of orders $n = 6$ and $n = 10$ have been taken into account. As an example, we have assumed that $R_0 = 0.8R$ and $T = 5000$ K initially. Light and shade in the picture correspond to the number of survived particles after 1000 rf periods; a larger number of particles can be trapped in darker area.

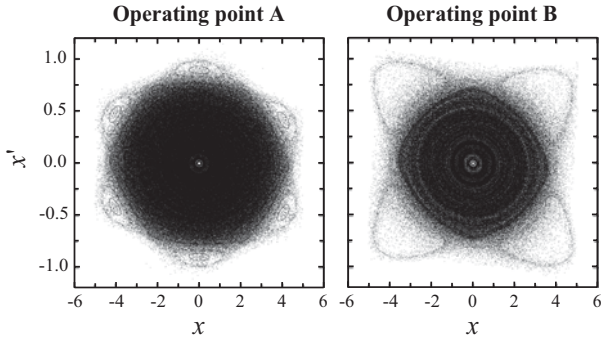

Fig. 4. Poincaré surface-of-section plots corresponding to the operating points A and B in Fig. 3.

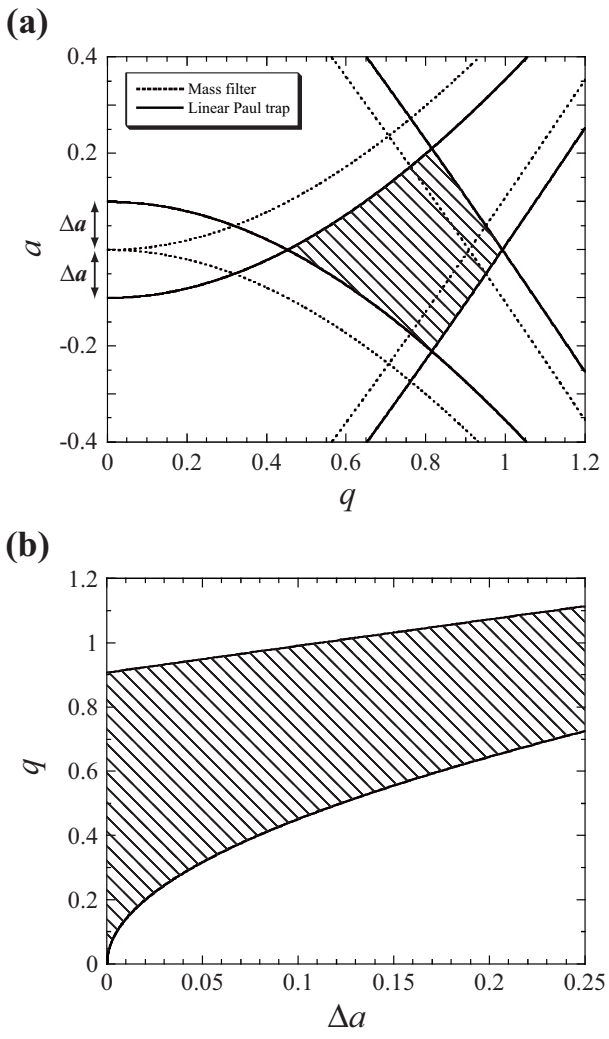

Fig. 5. Stability diagrams for a linear Paul trap. (a) The Mathieu stability region (the hatched area) of a linear Paul trap with a finite Δa. The original boundaries expected from the 2D mass-filter theory have been drawn with dotted lines. (b) The acceptable range of q on the $a = 0$ axis of the Mathieu diagram has been plotted as a function of Δa.

Unlike axially uniform mass filters, a linear Paul trap has an additional potential well to confine particles longitudinally. The longitudinal confinement is usually achieved by applying static potentials to thin electrodes at both ends of the quadrupole rods. The longitudinal confinement is accompanies by a radial defocusing effect according to the Earnshaw's theorem; in other words, the radial focusing is more or less weakened by the axial potential, which can be a source of discrepancy between the 2D theory and experimental observations.

Suppose that we have an rf quadrupole of axial length L. When L is comparable to the aperture size $2R$, the static potential generated by the end electrodes can be approximated as[3)]

$$\phi_{\rm dc}(x,y,z) = \frac{4\kappa U_{\rm end}}{L^2}\left[z^2-\frac{1}{2}(x^2+y^2)\right] = \frac{m}{2Q}\omega_z^2\left[z^2-\frac{1}{2}(x^2+y^2)\right] \quad (4)$$

where $U_{\rm end}$ is the static voltage applied to the end electrodes, $\omega_z \equiv \sqrt{8\kappa Q U_{\rm end}/(mL^2)}$ is the angular frequency of the axial particle oscillation, and κ is a constant factor depending on the trap geometry. κ is often deduced from the observed value of ω_z. In an axially long trap, the potentials of the end electrodes are shielded by the quadrupole rods, which makes the longitudinal potential well almost flat in the middle of the trap. It is, however, still possible to employ the approximate potential in eq. (4) if the plasma is localized around the trap center. Since eq. (4) contains transverse quadratic terms, adding this dc potential to the rf quadrupole potential leads to a shift of the a-parameter in eq. (3).[42,46)] The modified a-parameters are given by $a_x = a - \Delta a$ for x-

direction and $a_y = a + \Delta a$ for y-direction where $\Delta a \equiv 16\kappa Q U_{\rm end}/(mL^2\Omega^2)$. The characteristic exponents β_x and β_y that determine the secular frequencies of the particle oscillation are thus changed to $\tilde{\beta}_{x(y)} = \sqrt{\beta^2_{x(y)} - \Delta a}$ under the smooth approximation. As demonstrated in Fig. 5(a), the Mathieu stability region shrinks with a finite Δa. Figure 5(b) shows the stability range on the q-axis (i.e. along the $a = 0$ line) plotted as a function of Δa. We recognize that the acceptable range of q for particle stability becomes narrower as Δa increases. Needless to say, the transverse resonance conditions can also be influenced by the existence of the axial potential. The original lines in Fig. 1 are expected to shift to the high q side.

(ii) Mechanical errors

So far, the bias potential U and the quadrupole amplitude V are supposed to represent the exact voltages applied to the electrodes. These parameters in eq. (3) can be affected in practice by mechanical errors; field distortions due to misalignments of the electrodes and manufacture errors modify the amplitudes of all multipole-components. In particular, C_2 is deviated from unity, depending on the amount of errors.[45,47] To figure out the importance of this effect, we here take a simple example where only one of the four quadrupole rods is displaced from the ideal position.

Assume that four infinitely long cylindrical rods of radius $\rho = 5.75$ mm are symmetrically placed 5 mm away from the trap axis, so that $\rho/R = 1.15$. Neighboring rods have potentials with the same absolute value but opposite signs in order to excite a strong quadrupole field. We then radially displace one of the rods by the amount of ΔR mm. Under this boundary condition, we numerically integrate the Maxwell equations with the MAFIA code[48] to calculate the multipole potential in the central region. Since output data from MAFIA have a resolution limited by the mesh size, the least-square fitting is carried out before taking the multipole expansion. Figure 6 shows the magnitude of the quadrupole coefficient C_2 evaluated at the radial position $r = 4$ mm from the quadrupole field center. We find that the quadrupole strength is actually affected by mechanical errors and, in the present example, C_2 almost linearly depends on the rod displacement ΔR. The change of C_2 results in the shift of stop bands. The deviation of C_2 from unity is, however, not very serious as long as the trap is carefully constructed.

(iii) Coulomb interactions among confined particles

Provided that the density of the plasma is high, the single-particle picture described in the previous sections no longer applies but we have

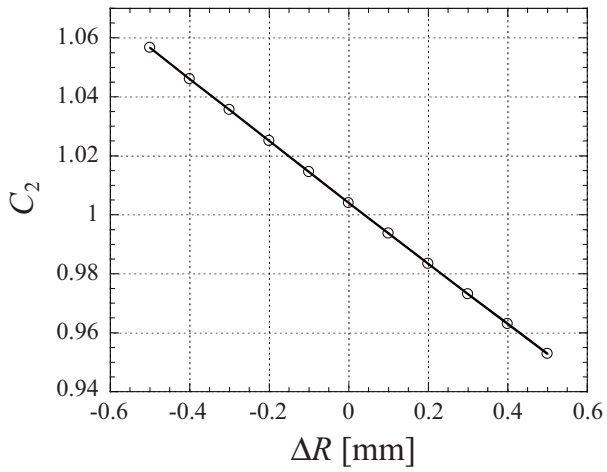

Fig. 6. Dependence of the quadrupole coefficient C_2 on the amount of the rod displacement ΔR.

to incorporate the effect of space-charge self-fields. Since the Coulomb forces among confined particles are repulsive, the secular frequencies are always depressed. Smoothing out the time-dependency of the Mathieu equation, we obtain in the absence of space charge $d^2x/dt^2 + \omega_x^2 x = 0$ where the secular frequency ω_x is given by $\omega_x = \Omega\sqrt{a + q^2/2}/2$. Recalling that the confined plasma is homogenized at high phase-space density due to the Debye screening, we assume, for the sake of simplicity, that the spatial distribution of charges is roughly uniform within a cylindrical region of radius r_0. The average Coulomb potential is then given by $\phi_{\rm sc} = -\lambda Q r^2/(4\pi\varepsilon_0 r_0^2)$ where λ is the line density of the plasma. The repulsive force reduces the secular frequency to $\tilde{\omega}_x = \sqrt{\omega_x^2 - \lambda Q^2/(2\pi\varepsilon_0 m r_0^2)}$, causing a shift of the resonance line in eq. (2). The amount of the shift certainly depends on the plasma density. The frequency reduction due to the collective Coulomb interactions is referred to as the *incoherent tune shift* in the beam-physics community. The ratio of the effective frequency to the original one, i.e. $\eta \equiv \tilde{\omega}_x/\omega_x$, is called the *tune depression* that tells us how strongly the beam is dominated by space charges. When the transverse temperature of a plasma in the linear trap is $T_\perp$, η can be estimated from[26]

$$\eta = \sqrt{1 - \frac{1}{1 + \dfrac{2}{\lambda r_{\rm p}} \dfrac{k_{\rm B} T_\perp}{mc^2}}} \qquad (5)$$

where $k_{\rm B}$ is the Boltzmann constant, c is the speed of light, and $r_{\rm p}$ denotes the classical particle radius. η ranges from 0 (low-temperature limit) to 1 (high-temperature limit).

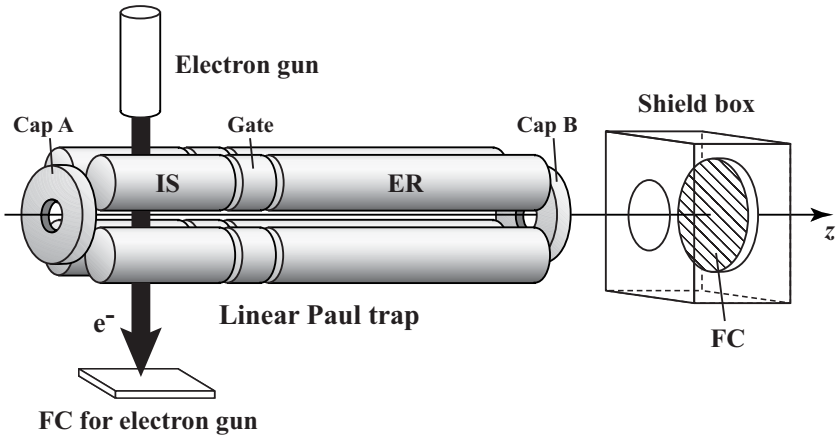

Fig. 7. Schematic view of the trap system. The linear Paul trap has been separated into three sections that are called "Ion Source (IS)", "Gate", and "Experiment Region (ER)". Dc voltages are applied to the end electrodes, i.e. "Cap A" and "Cap B", for axial plasma confinement.

3. Experiment

3.1 Setup

Figure 7 illustrates the experimental setup employed for our resonance study. All the components were arranged in a compact chamber where the vacuum pressure 3×10^{-8} Pa can be reached with a turbo-molecular pump. We utilized the multi-section linear Paul trap developed for S-POD. Since the details of the system have been described in ref. 28, we here only outline the basic parameters. Our trap is composed mainly of two planar electrodes and three sets of quadrupole rods (see Fig. 7). It is possible to form two potential wells along the axis by biasing the "Gate" quadrupole. Various ion plasmas can be produced in the "Ion Source (IS)" region beside which an electron gun and an atomic oven are placed. We can bring ions in IS to the "Experiment Region (ER)", if necessary, by switching off the bias voltage on the Gate electrodes. The lengths of IS, Gate, and ER are 50 mm, 9 mm, and 100 mm, respectively. For axial plasma confinement, dc voltages are applied to the two end electrodes called "Cap A" and "Cap B". Both caps are 5 mm in thickness and have a hole of 10 mmϕ. The quadrupole rods, all of which have a circular cross section of 5.75 mm in radius, i.e. $\rho = 5.75$ mm, are set 5 mm away from the trap axis, i.e. $R = 5.00$ mm. The frequency of the rf quadrupole field was fixed at 1 MHz, while its amplitude was taken as a variable to change the q parameter. The a parameter can be controlled by putting the dc potential U on the electrodes.

For the present purpose, $^{40}Ar^{+}$ plasmas generated by ionizing Ar gas with a low-energy electron beam were used. The Ar gas was introduced into the chamber until the pressure reached 5×10^{-6} Pa. We confined $^{40}Ar^{+}$ ions only in the IS region, keeping the Cap-B potential at the ground level. By shutting down the bias on Gate, the ions simply pass through ER toward the Faraday cup (FC) sitting 15 mm away from Cap B. The dc potential of Cap A was kept on at 30 V throughout the experiments. In order to improve the signal-to-noise (SN) ratio, we biased the IS quadrupole so that the ions are accelerated to FC. This procedure actually reduces the ion loss that occurs in the free space between Cap B and FC. When the accelerating bias is set at 10 V, the loss rate becomes less than 10% according to 3D simulations. We also covered FC with a grounded shield box to minimize the rf and switching noises. Typically, the electron gun was turned on for 5 s to make an $^{40}Ar^{+}$ plasma. After a 10-millisecond storage in IS, we shut down the bias potential on Gate to send the plasma toward the FC detector.

3.2 Results

3.2.1 Observation of nonlinear resonances

We first measured the number of output $^{40}Ar^{+}$ ions, scanning a wide area of the Mathieu stability diagram. Figure 8(a) shows a series of experimental observations obtained with various combinations of a and q. We find several local reductions of the output signals, which cannot be explained by the linear theory. It has been confirmed that these data are well reproducible. When $a = 0$, two apparent "dips" can be seen at $q \approx 0.45$ and 0.64. Each of them has gradually split into two dips as we increase a. The positions of these dips found in the experiments have been plotted on the (a, q)-space in Fig. 8(b). The open circles indicate the boundaries at which FC signals greater than the noise level started to appear (left end) or disappeared (right end). The solid and broken curves represent the nonlinear resonance lines predicted in Fig. 1. The results in Fig. 8 clearly demonstrate the existence of nonlinear resonances of orders $N = 4$ and 6. Considering the symmetry of the system, it is reasonable that the resonances of even orders are prominent. The slight shifts of the observed resonance points are most likely to originate from interparticle Coulomb interactions as clarified later. Figure 8 also suggests that coupling resonances are weak in our system.

In order to strengthen the above conclusion, numerical simulations were performed with a 3D particle tracking code that can take into account the exact trap geometry.[28] The MAFIA code was employed to calculate the 3D potential distribution in the trap for reliable simulations. We, however, ignored the Coulomb self-fields to

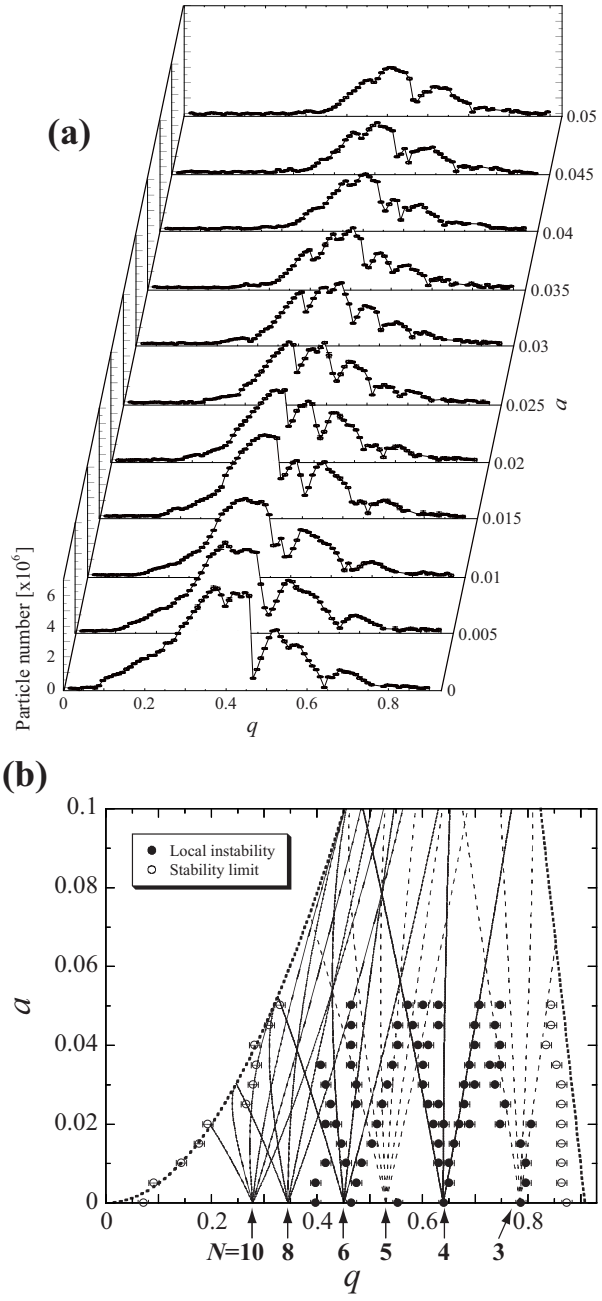

Fig. 8. Experimental results indicating the existence of nonlinear resonances in the linear Paul trap. (a) Number of $^{40}Ar^{+}$ ions detected by FC with various combinations of the Mathieu parameters a and q. The ion numbers were deduced from the strengths of the FC output signals. (b) Locations of the operating points at which the local reductions of FC signals were observed. The open circles show the stability boundaries expected from the present experiments.

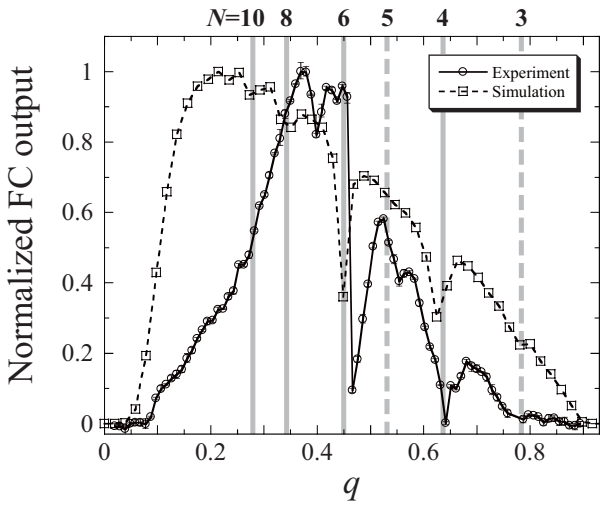

Fig. 9. Comparison of the experimental result for $a = 0$ with the corresponding tracking simulations. The ordinate represents the strength of FC signals normalized by the peak value. The vertical lines show the positions of nonlinear resonances predicted by the 2D theory in §2; the four solid lines correspond to even-order resonances while the two broken lines to odd-order resonances.

save the computing time. Typical simulation results obtained with $a = 0$ are plotted in Fig. 9 where we again observe two clear dips due to nonlinear resonances. Since no mechanical errors have been assumed in these simulations, the major source of the nonlinearity should be the non-hyperbolic surface of the quadrupole electrodes. The six vertical lines show the locations of resonance stop bands expected from the 2D theoretical model. It is now evident that the local instability at $q \approx 0.45$ can be attributed to the $N = 6$ resonance while the instability at $q \approx 0.64$ to the $N = 4$ resonance.

For comparison, the experimental data for $a = 0$ has been superimposed on the simulation result in Fig. 9. The dip positions are almost consistent to the numerical data except for a slight shift to the high q side. The discrepancy between the numerical and experimental power distributions is caused, e.g., by lack of information of the initial ion distribution. As already shown in Fig. 2, the number of output particles can vary depending on the initial plasma conditions. Since ions are continuously produced through the interactions with electrons almost everywhere in the confinement region, it is difficult to know the accurate ion distribution in six-dimensional phase space. In the present simulations, therefore, we took the same particle-generation procedure as adopted in ref. 28. The ion loss due to collisions with the other ions and residual gas atoms, which has not been incorporated in the simulations, could also reduce the strength of actual FC signals especially near the stability boundaries.

3.2.2 Space charge effect

We are now in a position to discuss the observed shift of the resonance lines. As pointed out in §2.3, some practical factors may modify the resonance condition (2) based on the ideal 2D model. Remember first that our tracking code uses the 3D potential distribution evaluated by MAFIA. The details of the trap configuration have been considered quite accurately; the effects of the axial confinement and even mechanical errors have been taken into account in the simulations here. Nevertheless, the dip locations in Fig. 9 are in excellent agreement with the 2D prediction. Although no mechanical errors have been assumed in the simulations of Fig. 9, the result turns out to be almost unchanged unless the trap contains unreasonably large imperfections. For instance, the shift of q due to error fields should be less than 1% in

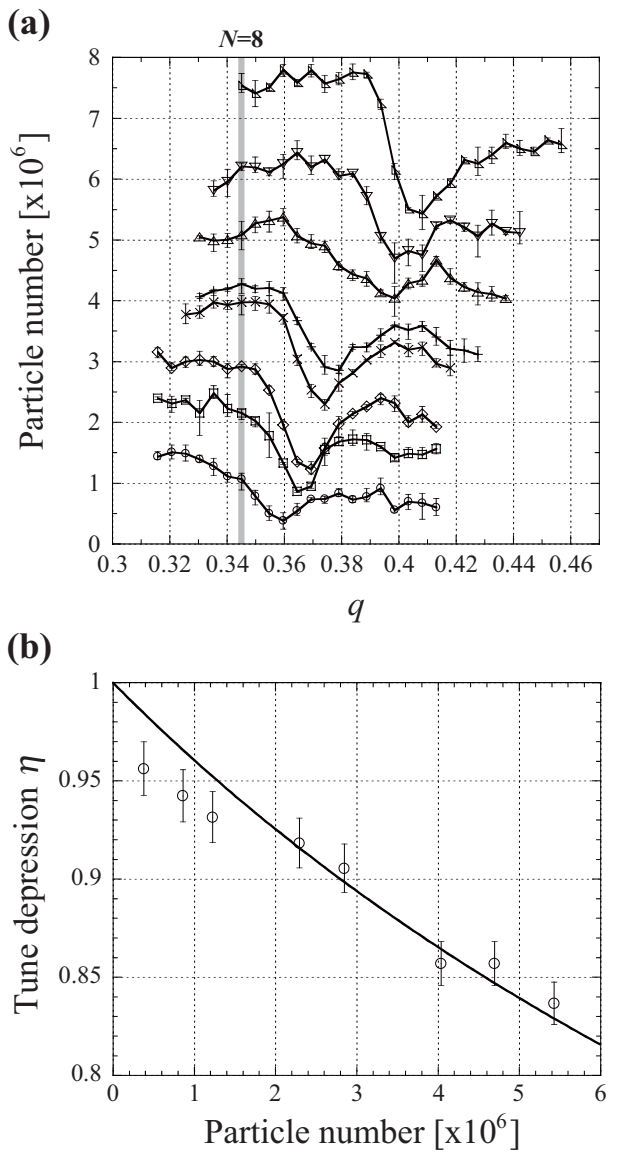

Fig. 10. Experimental results indicating the space charge effect on a resonance stop band. (a) FC outputs obtained in eight different series of experiments. The number of $^{40}Ar^{+}$ ions initially confined in the trap has been controlled in each series by changing the current of the ionizing electron beam. The vertical line shows the location of the $N = 8$ resonance expected from the 2D mass filter theory. (b) Tune depression estimated from the observed shift of the $N = 8$ resonance. The solid line is obtained from eq. (5) by fitting the experimental results.

our Paul trap according to Fig. 6. After all, the discrepancy between the experimental and numerical resonance conditions cannot be explained by the first two factors described in §2.3.

The most probable cause of the resonance shift is the Coulomb potential. Considering that the interparticle Coulomb force is repulsive, the resonance lines should move to the high-q side, which is consistent to the observations in Figs. 8 and 9. If the Coulomb potential is really responsible for the effect, the positions of the local instability must depend on the charge density of the plasma. It is worthy to recognize that, in Fig. 8(b), the deviation from a theoretical resonance line is greater for the $N = 6$ resonance rather than for the $N = 4$ resonance; this is probably because the number of ions initially confined in the trap is peaked near $q \approx 0.4$ and then, rapidly decreases at a higher q [see Figs. 8(a) and 9]. To look into density-dependent effects systematically, we carried out experiments controlling the total number of confined ions. The ion number can be changed by adjusting the current of the electron beam from the gun. Since the space charge effect appears more clearly at higher density, we here pay attention to the $N = 8$ resonance that occurs near the peak of FC output signals. Figure 10(a) summarizes the results of experiments where eight different electron currents have been employed. As expected, the local resonant instability is encountered at a higher q as the initial number of ions becomes larger. We also notice that the width of the dip tends to be wider at higher ion density. In order to make a rough estimate of the tune depression η from these data, we state that the $N = 8$ resonance line has moved in each series of experiments from $q \approx 0.345$ to the point at which the FC output was minimized. η can then be evaluated by taking the ratio of the secular frequencies corresponding to $q \approx 0.345$ and the observed minimum. The result has been shown in Fig. 10(b).

It is possible to evaluate the tune depression from eq. (5) under some assumptions. According to preliminary data, the longitudinal temperature $T_{\parallel}$ grows steadily until the number of ions reaches about 2×10^6, and then comes to a plateau where $T_{\parallel} \approx 0.28$ eV. A MAFIA calculation of the potential well along the trap axis suggests that the longitudinal plasma extent L_0 corresponding to this temperature is approximately 31 mm. By assuming that L_0 is maintained once the ion number exceeds 2×10^6, we can make a rough estimate of the line density λ. On the other hand, the transverse temperature $T_{\perp}$ is sensitive to the Mathieu parameter q rather than the number of confined ions because the energy gain from the rf field is so large. We thus anticipate that, in such a narrow range of q as considered in Fig. 10(a), $T_{\perp}$ should be almost constant. The solid curve in Fig. 10(b) was obtained by assuming that $L_0 \approx 31$ mm and $T_{\perp} \approx 0.28$ eV. It is quite reasonable that the best fit of the experimental points was achieved with this transverse temperature equal to the observed longitudinal temperature.

4. Summary

We have explored the effects of nonlinear resonances in a linear Paul trap through systematic experiments and numerical simulations. 2D tracking simulations were performed to study the efficiency of plasma storage with or without multipole error fields. It has been shown that the storage efficiency depends on the initial conditions of the plasma even when no field imperfections are included in the system. We have also confirmed that the conventional mass-filter theory explains the local instability due to nonlinear resonances caused by mechanical errors.

A linear Paul trap developed for S-POD was employed to observe nonlinear resonances experimentally. A large number of $^{40}Ar^{+}$ ions were confined in the trap operated with various combinations of the Mathieu parameters a and q. Clear local instability was found in the vicinity

of resonance lines predicted by the 2D theory. As expected, a couple of even-order nonlinear resonances were particularly strong. The primary source of the nonlinearity in our system is believed to be the non-hyperbolic surface of the quadrupole electrodes. Slight shifts of the resonance lines from the theoretically predicted positions were observed which suggests the reduction of the secular frequency due to the interparticle Coulomb interactions. Controlling the number of confined ions in the trap, we demonstrated the dependence of nonlinear resonance conditions on the plasma density. The maximum tune depression achieved in the present experiments has been estimated to be $\eta \approx 0.84$.

Acknowledgements

The authors are indebted to Dr. Okabe for developing the 3D tracking code. They also thank Dr. Yoshimoto for his assistance in running the MAFIA code. This work was supported in part by a Grant-in-Aid for Scientific Research from the Ministry of Education, Culture, Sports, Science and Technology.

1) W. Paul and H. Steinwedel: Z. Naturforsch. A **8** (1953) 448.
2) J. D. Prestage, G. J. Dick and L. Maleki: J. Appl. Phys. **66** (1989) 1013.
3) M. G. Raizen, J. M. Gilligan, J. C. Bergquist, W. M. Itano and D. J. Wineland: Phys. Rev. A **45** (1992) 6493.
4) D. J. Berkeland, J. D. Miller, J. C. Bergquist, W. M. Itano and D. J. Wineland: Phys. Rev. Lett. **80** (1998) 2089.
5) R. B. Warrington, P. T. H. Fisk, M. J. Wouters and M. A. Lawn: IEEE Trans. Ultrason. Ferroelectr. Freq. Control **49** (2002) 1166.
6) K. Okada, M. Wada, T. Nakamura, R. Iida, S. Ohtani, J. Tanaka, H. Kawakami and I. Katayama: J. Phys. Soc. Jpn. **67** (1998) 3073.
7) K. Matsubara, U. Tanaka, H. Imajo, S. Urabe and M. Watanabe: Appl. Phys. B **76** (2003) 209.
8) T. Baba and I. Waki: Jpn. J. Appl. Phys. **35** (1996) L1134.
9) Y. Kai, K. Toyoda, M. Watanabe and S. Urabe: Jpn. J. Appl. Phys. **40** (2001) 5136.
10) M. Welling, H. A. Schuessler, R. I. Thompson and H. Walther: Int. J. Mass Spectrom. Ion Processes **172** (1998) 95.
11) M. Drewsen, I. Jensen, J. Lindballe, N. Nissen, R. Martinussen, A. Mortensen, P. Staanum and D. Voigt: Int. J. Mass Spectrom. **229** (2003) 83.
12) K. Okada, M. Wada, T. Nakamura, T. Takayanagi, I. Katayama and S. Ohtani: Jpn. J. Appl. Phys. **45** (2006) 956.
13) D. G. Enzer, M. M. Schauer, J. J. Gomez, M. S. Gulley, M. H. Holzscheiter, P.G. Kwiat, S. K. Lamoreaux, C. G. Peterson, V. D. Sandberg, D. Tupa, A. G. White, R. J. Hughes and D. F. V. James: Phys. Rev. Lett. **85** (2000) 2466.
14) M. Block, A. Drakoudis, H. Leuthner, P. Seibert and G. Werth: J. Phys. B-At. Mol. Opt. Phys. **33** (2000) L375.
15) L. Hornekær and M. Drewsen: Phys. Rev. A **66** (2002) 013412.
16) J. I. Cirac and P. Zoller: Phys. Rev. Lett. **74** (1995) 4091.
17) A. Steane: Appl. Phys. B **64** (1997) 623.
18) R. J. Hughes, D. F. V. James, J. J. Gomez, M. S. Gulley, M. H. Holzscheiter, P. G. Kwiat, S. K. Lamoreaux, C. G. Peterson, V. D. Sandberg, M. M. Schauer, C. M. Simmons, C. E. Thorburn, D. Tupa, P. Z. Wang and A. G. White: Fortschr. Phys. **46** (1998) 329.
19) H. C. Nägerl, Ch. Roos, D. Leibfried, H. Rohde, G. Thalhammer, J. Eschner, F. Schmidt-Kaler and R. Blatt: Phys. Rev. A **61** (2000) 023405.
20) D. Leibfried, B. DeMarco, V. Meyer, M. Rowe, A. Ben-Kish, M. Barrett, J. Britton, J. Hughes, W. M. Itano, B. M. Jelenković, C. Langer, D. Lucas, T. Rosenband and D. J. Wineland: J. Phys. B-At. Mol. Opt. Phys. **36** (2003) 599.
21) D. M. Lucas, C. J. S. Donald, J. P. Home, M. J. McDonnell, A. Ramos, D. N. Stacey, J. P. Stacey, A. M. Steane and S. C. Webster: Phil. Trans. R. Soc. Lond. A **361** (2003) 1401.
22) F. Schmidt-Kaler, H. Häffner, S. Gulde, M. Riebe, G. P. T. Lancaster, T. Deuschle, C. Becher, W. Hänsel, J. Eschner, C. F. Roos and R. Blatt: Appl. Phys. B **77** (2003) 789.
23) T. Furukawa, J. Nishimura, U. Tanaka and S. Urabe: Jpn. J. Appl. Phys. **44** (2005) 7619.
24) H. Okamoto: Hiroshima Univ. Rep. HUBP-01/98, 1998.
25) H. Okamoto and H. Tanaka: Nucl. Instrum. Methods Phys. Res., Sect. A **437** (1999) 178.
26) H. Okamoto, Y. Wada and R. Takai: Nucl. Instrum. Methods Phys. Res., Sect. A **485** (2002) 244.
27) R. Takai, K. Ito, Y. Iwashita, H. Okamoto, S. Taniguchi and Y. Tomita: Nucl. Instrum. Methods Phys. Res., Sect. A **532** (2004) 508.
28) R. Takai, H. Enokizono, K. Ito, Y. Mizuno, K. Okabe and H. Okamoto: Jpn. J. Appl. Phys. **45** (2006) 5332.
29) F. von Busch and W. Paul: Z. Phys. **164** (1961) 588.
30) P. H. Dawson and N. R. Whetten: Int. J. Mass Spectrom. Ion Phys. **2** (1969) 45.
31) F. Guidugli and P. Traldi: Rapid Commun. Mass Spectrom. **5** (1991) 343.
32) K. L. Morand, S. A. Lammert and R. G. Cooks: Rapid Commun. Mass Spectrom. **5** (1991) 491.
33) F. Guidugli, P. Traldi, A. M. Franklin, M. L. Langford, J. Murrell and J. F. J. Todd: Rapid Commun. Mass Spectrom. **6** (1992) 229.
34) D. M. Eades and R. A. Yost: Rapid Commun. Mass Spectrom. **6** (1992) 573.
35) Y. Wang, J. Franzen and K. P. Wanczek: Int. J. Mass Spectrom. Ion Processes **124** (1993) 125.
36) Y. Wang: Rapid Commun. Mass Spectrom. **7** (1993) 920.
37) D. M. Eades, J. V. Johnsen and R. A. Yost: J. Am. Soc. Mass Spectrom. **4** (1993) 917.
38) R. Alheit, C. Hennig, R. Morgenstern, F. Vedel and G. Werth: Appl. Phys. B **61** (1995) 277.
39) R. Alheit, S. Kleineidam, F. Vedel, M. Vedel and G. Werth: Int. J. Mass Spectrom. Ion Processes **154** (1996) 155.
40) T. Gudjons, P. Seibert, G. Werth: Appl. Phys. B **65** (1997) 57.
41) T. Mori, K. Toyoda, M. Watanabe and S. Urabe: Rev. Laser Eng. **31** (2003) 477 [in Japanese].
42) A. Drakoudis, M. Söllner and G. Werth: Int. J. Mass Spectrom. **252** (2006) 61.
43) G. E. Lee-Whiting and L. Yamazaki: Nucl. Instrum. Methods **94** (1971) 319.
44) A. J. Reuben, G. B. Smith, P. Moses, A. V. Vagov, M. D. Woods, D. B. Gordon and R. W. Munn: Int. J. Mass Spectrom. Ion Processes **154** (1996) 43.
45) D. J. Douglas and N. V. Konenkov: Rapid Commun. Mass Spectrom. **16** (2002) 1425.
46) M. Drewsen and A. Brøner: Phys. Rev. A **62** (2000) 045401.
47) S. Sevugarajan and A. G. Menon: Int. J. Mass Spectrom. **218** (2002) 181.
48) The MAFIA Collaboration: MAFIA Manual Version 4.024, CST GmbH, Darmstadt, 2000.